Efficient Preparation of Dicke States

Jeffery Yu,[1,2,3] Sean R. Muleady,[1,2,*] Yu-Xin Wang (王语馨),[1,*] Nathan Schine,[2,3]
Alexey V. Gorshkov,[1,2] and Andrew M. Childs[1,4]
[1]Joint Center for Quantum Information and Computer Science,
NIST/University of Maryland, College Park, Maryland 20742, USA
[2]Joint Quantum Institute, NIST/University of Maryland, College Park, Maryland 20742, USA
[3]Department of Physics, University of Maryland, College Park, Maryland 20742, USA
[4]Department of Computer Science and Institute for Advanced Computer Studies,
University of Maryland, College Park, Maryland 20742, USA

(Received 10 January 2025; revised 28 August 2025; accepted 24 October 2025; published 20 January 2026)

We present an algorithm utilizing midcircuit measurement and feedback that prepares Dicke states with polylogarithmically many ancillae and polylogarithmic depth. Our algorithm uses only global midcircuit projective measurements and adaptively chosen global rotations. This improves over prior work that was only efficient for Dicke states of low weight or was not efficient in both depth and width. Our algorithm can also naturally be implemented in a cavity QED context using logarithmic time, zero ancillae, and atom-photon coupling scaling with the square root of the system size.

DOI: 10.1103/9gjk-rgql

The controlled preparation of entangled states is a central goal in quantum science, with broad implications for tasks in quantum information, sensing, and many-body physics. Dicke states are a particularly important and well-studied class of entangled state [1], where the weight-w Dicke state consists of a symmetric superposition of n qubits with a fixed number w of spin flips. Such states are total angular momentum eigenstates, feature prominently in the study of superradiance in quantum optics [1], and also appear in condensed matter as ground states of paradigmatic models for quantum magnetism [2–4].

In recent years, Dicke states have gained prominence as a versatile resource for quantum information science, particularly for quantum sensing where they can achieve Heisenberg-limited scaling while offering robustness against erasures and other specific types of decoherence compared to Greenberger-Horne-Zeilinger states [5–13]. Dicke states have also been proposed as key components of quantum optimization algorithms [14–18], various quantum memory and error correction applications [19,20], and algorithms for preparing the ground states of integrable quantum systems [21]. Beyond this, Dicke states have also emerged as a practical test bed for wide-ranging applications, including quantum tomography [22] and quantum networking [23], owing to their high symmetry and multipartite nature.

Yet, despite their theoretical simplicity, efficient preparation of Dicke states, particularly on noisy intermediate-scale quantum devices [24] remains an outstanding challenge and a roadblock to their widespread application. Existing protocols for preparing Dicke states include both abstract circuit-based approaches [14,25–34] and more practical, tailored approaches for current and near-term experiments [8,13,23,35–49]. While some existing methods achieve low depth for low-weight states, efficient preparation of arbitrary-weight states, especially those with near-maximal entanglement ($w \approx n/2$), remains elusive. In particular, prior circuit-based approaches require either depths of $\Omega(n^{1/4})$ or otherwise use polynomially many ancilla qubits to achieve logarithmic depth across all weights [30,50].

Here, we develop an algorithm to prepare arbitrary-weight Dicke states, guided by nascent experimental capabilities, namely, midcircuit collective J_z measurements and global rotations, that provably achieves both polylogarithmic depth and ancilla count for the first time. Prior work in cavity quantum electrodynamics has explored how such measurements may be heralded by cavity photons or be used in continuous-measurement-and-feedback schemes to generate complex many-body entangled states [46,52–60]. Using these ideas, we propose a constant-time implementation of a J_z measurement in cavity systems. In the circuit model, this measurement can be implemented in polylogarithmic depth [31,61,62], adding only minimal overhead.

The algorithm is conceptually simple. Starting from the all spin-up state, we identically rotate each spin, followed by a collective J_z measurement, which projects onto a Dicke state. If we measure the desired weight w, we are done. If we measure some other w', we rotate again by some angle conditioned on w', perform another measurement, and repeat until we obtain w. The choice of rotation angles is motivated by an intuitive geometric phase-space representation on the

*These two authors contributed equally to this work.

collective Bloch sphere. We demonstrate that only logarithmically many iterations of measurement and feedback suffice to prepare *any* desired Dicke state, with a rigorous proof for the presumable worst case of $w = n/2$. We also demonstrate the robustness of our algorithm to typical error sources relevant for cavity-based measurement schemes.

Beyond its efficiency, our algorithm's conceptual simplicity and natural suitability for atom-cavity systems opens the door to implementation in near-term quantum sensors. Cavity-based sensors have already harnessed entangled spin-squeezed states for metrological quantum advantage [63], while also demonstrating pioneering studies at the forefront of precision metrology and fundamental science [64]. Our algorithm thus offers a pathway toward further improvements in sensitivity for such fundamental studies [65–70], where $w = n/2$ Dicke states offer even greater enhancements to sensitivity, close to the ultimate limits imposed by quantum mechanics.

Preliminaries—Dicke states have a convenient representation in terms of angular momentum eigenstates, where the n qubits are viewed as spin-$\frac{1}{2}$ particles. Let $\mathbf{S}_k$ be the angular momentum operator for the kth qubit, and let $\mathbf{J} = \sum_{k=1}^{n} \mathbf{S}_k$ be the total angular momentum operator. The Dicke states $|j, m\rangle$ are the simultaneous eigenstates of $\mathbf{J}^2$ and J_z with quantum numbers $j = (n/2)$ and $m \in \{-j, -j+1, \ldots, j\}$, respectively. The Dicke state $|j, m\rangle$ is a uniform superposition of states with fixed z magnetization m or, equivalently, strings of $n = 2j$ bits with Hamming weight $w = j - m$. These states are invariant under permutations of the qubits.

We assume the following primitives for our model of computation: (1) prepare $|0\rangle^{\otimes n}$ states on demand, (2) perform collective rotations (uniform single-qubit gates) about the y axis, and (3) perform J_z measurements. Note that both collective rotations, expressed via the unitary $e^{-i\theta J_y}$, and J_z measurements preserve the total angular momentum $\mathbf{J}^2$, leaving the quantum number $j = (n/2)$ fixed.

Below, we present an experimental setup where a collective J_z measurement can be implemented in $O(1)$ time, independent of n. Even without access to collective measurements, we can implement a J_z measurement in the ordinary circuit model, where such a measurement is equivalent to a projective Hamming weight measurement, with only polylogarithmic overhead in n. One approach is to set $\lfloor \log(n) \rfloor + 1$ ancillae to be the measurement register and accumulate the Hamming weight into those qubits. Reference [61] gives an implementation of this in $O(\log^2 n)$ depth with no additional ancillae.

Algorithm—Our goal is to prepare the Dicke state $|j, m_t\rangle$ for a desired target value of m_t, starting from the initial product state $|j, j\rangle = |0\rangle^{\otimes n}$. The basic algorithm is to perform a uniform rotation $e^{-i\theta J_y}$ for some angle θ and measure J_z. If $m = m_t$ is measured, we are done; otherwise, we iterate this procedure, choosing subsequent rotation angles θ based on the prior outcome of the measurement of J_z.

A natural strategy is to adaptively choose the rotation angles θ to maximize the overlap of the current state with the target Dicke state on each iteration of the algorithm. Since both the initial state and the state following each collective J_z measurement are of the form $|j, m\rangle$, we let $\theta = \theta_{m_t,m}$, where $\theta_{m_t,m}$ approximately maximizes the quantity

$$\left|d^{j}_{m_t,m}(\theta_{m_t,m})\right|^2 = \left|\langle j, m_t | e^{-i\theta_{m_t,m} J_y} | j, m\rangle\right|^2, \tag{1}$$

where $d^{j}_{m_t,m}(\theta)$ are known as elements of the Wigner d matrix.

To specify a suitable set of angles $\theta_{m_t,m}$ and to understand the properties of our algorithm, we find it useful to first visualize the Dicke states in terms of their phase-space distributions. In particular, consider the Husimi Q distribution $Q(\theta, \phi) = |\langle \psi | \theta, \phi\rangle|^2/\pi$ for a state $|\psi\rangle$, where $|\theta, \phi\rangle = e^{-i\phi J_z} e^{-i\theta J_y} |j, j\rangle$ is a coherent spin state oriented along an axis $\mathbf{n}$ with polar and azimuthal angles θ and ϕ, respectively [71]. We can thus geometrically map the Q distribution for a state onto the surface of a collective Bloch sphere with radius j. The Q distribution for the Dicke state $|\psi\rangle = |j, m\rangle$ is $Q_m(\theta, \phi) = (1/\pi)\binom{2j}{j+m} \cos^{2(j+m)}(\theta/2) \sin^{2(j-m)}(\theta/2)$. On the collective Bloch sphere surface, as $j \to \infty$, these correspond to narrow horizontal rings of radius $r_m = \sqrt{j^2 - m^2}$ located at a height m above the equator for $m \neq |j|$; for $m = \pm j$, this instead corresponds to a narrow Gaussian distribution at either pole [72,73]. For a uniform rotation of $|j, m\rangle$ via $e^{-i\theta J_y}$, the Q distribution undergoes the analogous rotation on the collective Bloch sphere. This results in a "tilted ring" distribution, where the normal vector to the plane of the ring forms an angle θ to the z axis.

Within this geometric picture, a reasonable choice of angle $\theta_{m_t,m}$ is one that maximizes the overlap of the Q distributions of the rotated state and the target Dicke state in the limit of large j. This maximum occurs when the corresponding ring distributions intersect at a point sharing the same tangent vector, as shown in Fig. 1. This condition is met for rotation angle

$$\theta_{m_t,m} = \arcsin\left[(m r_{m_t} - m_t r_m)/r_0^2\right]. \tag{2}$$

This offers an analytically simple choice of angle for our algorithm, without the need to resort to numerical optimization of Eq. (1). In the End Matter, we argue that our algorithm and choice of angle in Eq. (2) generically prepare arbitrary target Dicke states in time $O[\log(j - |m_t|)]$. In particular, we predict that the running time decreases with increasing $|m_t|$, which is consistent with numerical calculations discussed below.

We now focus on the specific case of $m_t = 0$, corresponding to the Dicke state with maximal interspin

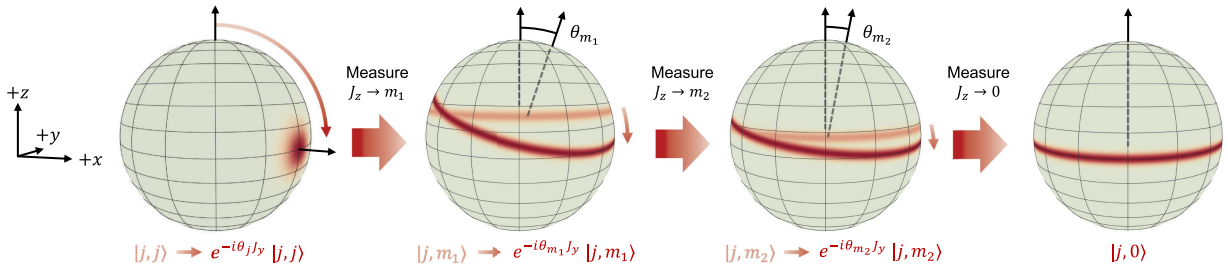

FIG. 1. A geometric representation of our algorithm using the Husimi Q distribution for the Dicke states, represented as rings on the collective Bloch sphere. For each iteration i, the algorithm rotates the current state (depicted by the lighter ring) $|j,m_i\rangle$ by angle θ_{m_i} about $+y$, so that the resulting (darker) ring is tangent to the ring of the target Dicke state, maximizing their overlap. For a target $m_t = 0$, the corresponding ring lies at the Bloch sphere equator. We project with a J_z measurement and repeat until we measure the desired state.

entanglement and which exhibits the worst-case performance over all choices of m_t. Then Eq. (2) reduces to $\theta_m \equiv \theta_{0,m} = \arcsin(m/j)$. The transition probabilities $\mathrm{Prob}[m \to m'] = |d^j_{m',m}(\theta_m)|^2$ are the probabilities of measuring $|j,m'\rangle$ after rotating by θ_m from state $|j,m\rangle$ and are plotted in Fig. 2. We see in Fig. 3(a) that our choice of θ_m is numerically close to the optimal θ^*_m that maximizes Eq. (1).

As shown in Fig. 2 and its inset, there are some m for which $|d^j_{0,m}(\theta_m)|^2 < |d^j_{0,j}(\theta_j)|^2$; i.e., we have a lower probability of reaching the $m = 0$ state with the optimal rotation than if we start over with $m = j$ and rotate by $(\pi/2)$. In these cases, we choose to reset all qubits to $|0\rangle$ and restart from $m = j$. Empirically, we observe this to hold for $|m| \gtrsim j^{3/4}$. Though there is negligible difference in the numerical run-time, we include this reset whenever $|m| > j^{1/2}$ for ease of the formal proof in Supplemental Material [74].

Run-time analysis—In this section, we sketch our proof of the run-time for $m_t = 0$. The full calculations are provided in Supplemental Material [74]. We consider each iteration of global rotations and J_z measurements to take unit time.

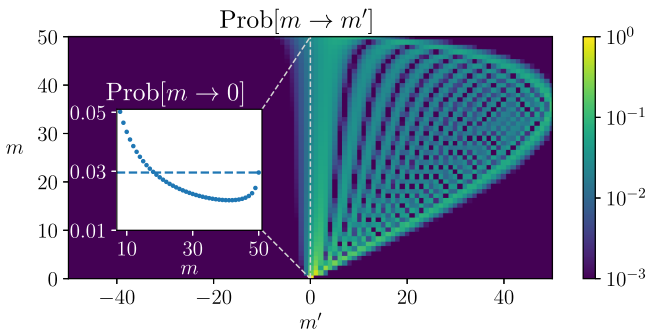

FIG. 2. For $j = 50$ and $m_t = 0$, transition probability matrix $\mathrm{Prob}[m \to m']$ of the base algorithm without resets, which is symmetric about the origin, i.e., $\mathrm{Prob}[-m \to -m'] = \mathrm{Prob}[m \to m']$. Inset: transition probabilities for the $m' = 0$ slice, which shows that for some m it is more advantageous to reset to $m = j$.

Theorem 1—The Dicke state $|j,0\rangle$ can be prepared in expected $O(\log j)$ time.

At a high level, our strategy is to show that, for some constant exponent $\alpha > 0$, the expectation value $\langle |m(t)|^\alpha \rangle$ over random measurement outcomes decays to 0 exponentially in time t. This means that, given any $\varepsilon > 0$, we can achieve $\langle |m(t)|^\alpha \rangle < \varepsilon$ within logarithmic time. Since the values of m are discretized, if $\langle |m(t)|^\alpha \rangle < \varepsilon$, then the probability of being in the $m = 0$ state after t steps is $\mathrm{Prob}[m(t) = 0] > 1 - \varepsilon$, as shown in Supplemental Material [74].

First, we show that starting from the initial $m = j$ state, we can obtain $|m| \le \sqrt{j}$ in expected $O(1)$ time. This follows since the measurement outcomes are binomially distributed around $m = 0$, and we obtain a measurement within a standard deviation with constant probability. As such, we introduce an additional reset step into the algorithm that takes any transient state with $|m| > \sqrt{j}$ back to $|j,j\rangle$, without impacting the scaling of the final run-time. We therefore utilize a proxy variable $M := \min(|m|, \sqrt{j} + 1)$. This still has the desirable property that if $\langle M(t)^\alpha \rangle < \varepsilon$, then the probability of reaching $m = 0$ after $O(t)$ steps is at least $1 - \varepsilon$.

In what follows, we show that it takes $O(\log j)$ steps to reach a state with $1 \ll m \ll \sqrt{j}$. As it takes $O(1)$ time to go from a state with $m \ll \sqrt{j}$ to the target $m = 0$, we thus prove that the overall run-time of our algorithm is $O(\log j)$. Using asymptotic expansions we derive for the Wigner d-matrix elements when $1 \ll m \ll \sqrt{j}$, we prove that there exists a constant $c < 1$ such that, for every m, we have $\sum_{m'=0}^{2m} |d^j_{m',m}(\theta_m)|^2 (M^\alpha / M'^\alpha) < c$, where M' is defined as a proxy for m' analogous to M (see Supplemental Material [74] for details). This implies that $[\langle M(t+1)^\alpha \rangle / \langle M(t)^\alpha \rangle] < c$ for each t, so $\langle M(t)^\alpha \rangle < c^t \langle M(0)^\alpha \rangle = c^t (\sqrt{j} + 1)^\alpha$. Therefore, for any desired $\varepsilon > 0$, we can attain $\langle M(t)^\alpha \rangle < \varepsilon$ with

$$t = \frac{\alpha \log(\sqrt{j} + 1) + \log(1/\varepsilon)}{\log(1/c)} = O(\log j) \tag{3}$$

steps, as claimed.

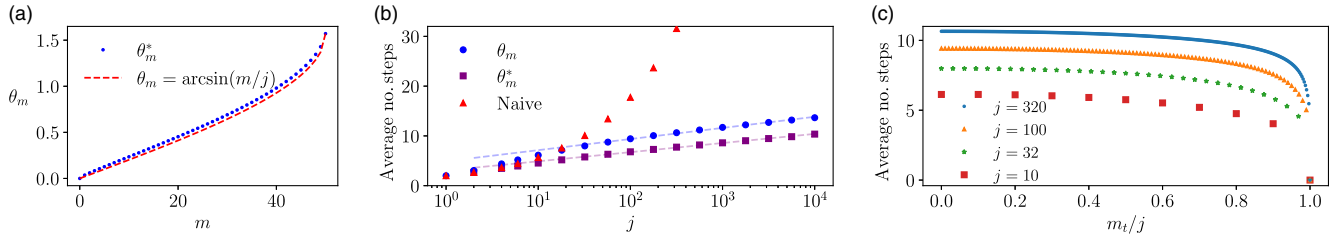

FIG. 3. (a) For $j = 50$ and $m_t = 0$, comparison of our chosen angles $\theta_m = \arcsin(m/j)$ and the numerically computed angles θ_m^* that maximize the overlap probability in Eq. (1). (b) Expected running time for preparing the $m_t = 0$ state with various algorithms. Our algorithm with θ_m (blue circles) exhibits similar logarithmic scaling as compared to using the numerically optimized angles θ_m^* (purple squares), both of which are exponentially faster than the polynomial running time with a naive approach of resetting at every step (red triangles). (c) Expected run-time of our algorithm, without resets, for arbitrary target states $|j, m_t\rangle$ using the angles in Eq. (2). In all cases, the preparation time decreases monotonically with $|m_t|$.

Numerics—Our algorithm can be understood as a discrete-time Markov chain with $2j + 1$ states corresponding to $m \in \{-j, -j + 1, \ldots, j\}$. The transition probabilities can be arranged into a stochastic matrix P, where P_{ab} is the probability of transitioning from the ath to the bth state. A visualization of P is shown in Fig. 2.

This is an absorbing Markov chain with the single absorbing state $m = 0$. The average number of steps before absorption can be calculated directly from P [82]. Figure 3(b) numerically compares the performance of our algorithm with variations in the choice of angles. In particular, our geometrically motivated angles $\theta_m = \arcsin(m/j)$ perform slightly worse than the optimal angles θ_m^*, but exhibit the same logarithmic scaling for the expected number of steps, with a relatively small constant prefactor, outperforming the naive approach of resetting after every step if unsuccessful.

Finally, in Fig. 3(c), we examine the preparation of Dicke states with arbitrary m_t, utilizing our choice of angles θ_{m,m_t} in Eq. (2). For various fixed j, we observe that this choice of angle results in an average number of steps strictly less than that required for the $m_t = 0$ case. We argue in the End Matter that this behavior is expected and that the corresponding average number of steps scales as $O[\log(j - |m_t|)]$.

Experimental considerations—Collective Hamming weight measurements may be directly implemented on an ensemble of n atomic qubits in which one of the two qubit states is coupled to a single-mode cavity. We illustrate this by considering three-level atoms as depicted in Fig. 4(a), with states $\{|0\rangle, |1\rangle, |e\rangle\}$, where $|0\rangle$ and $|1\rangle$ are the computational subspace and the cavity dispersively couples $|1\rangle$ to $|e\rangle$, i.e., with a large detuning between the cavity frequency and the atomic transition frequency between $|1\rangle$ and $|e\rangle$. Collective J_y rotations on the $|0\rangle - |1\rangle$ transition are straightforwardly performed via, e.g., variable-time microwave or optical pulses on neutral atomic qubits. [53,56,63,83–87]. In the rotating frame of a bare cavity photon (at laboratory frame frequency ω_c), the atom-cavity interaction Hamiltonian is

$$H = a^\dagger a \sum_{k=1}^{n} \frac{g^2}{\delta_k} \mathcal{P}_k, \tag{4}$$

where $a^\dagger$ (a) creates (annihilates) a cavity photon, $2g$ is the single-photon Rabi frequency, δ_k is detuning of the kth atom from the cavity, and $\mathcal{P}_k = \frac{1}{2}[I - 2(\mathbf{S}_k)_z]$. For our application, we set all detunings to be equal, i.e., $(g^2/\delta_k) = \chi$ for all k for some constant χ. Thus, the total cavity shift is $\Delta_a = \chi\mathcal{P}$, where $\mathcal{P} = \sum_k \mathcal{P}_k$, and the laboratory frame cavity transmission spectrum is $T(\omega) = \{\kappa^2/[4(\omega - \omega_c - \Delta_a)^2 + \kappa^2]\}$, where κ is the cavity linewidth and ω is the angular frequency of the cavity probe.

To ensure that all possible Hamming weights are accessible by a single monochromatic probe of the cavity, we require that the maximum total cavity shift is sufficiently small, i.e., $\chi n \ll \kappa$. This determines the atom-cavity detuning δ_k. We then probe on the side of the transmission peak, as depicted in Fig. 4(a), taking $\omega - \omega_c = \kappa/2$, to yield a Fisher information of $\mathcal{I}(\Delta_a) = [\kappa^2/(\kappa^2/2 - \kappa\Delta_a + \Delta_a^2)^2]$ for a single photon. The Cramér-Rao bound then gives $\mathrm{Var}(\tilde{\Delta}_a) \geq [1/\mathcal{I}(\Delta_a)] = [(\kappa/2) - \Delta_a + (\Delta_a^2/\kappa)]^2 \sim \kappa^2$ for any unbiased estimator $\tilde{\Delta}_a$ of Δ_a. Averaging over N photons and taking $\mathcal{P} = (\Delta_a/\chi)$ gives $\mathrm{Var}(\tilde{P}) \sim (1/N)(\kappa/\chi)^2$. We ensure that this variance is $O(1)$ by taking $N \sim (\kappa/\chi)^2 \propto n^2$ photons.

This scheme is straightforward, and the assumption of small total cavity shift is easy to satisfy experimentally. However, the number of photons required is quite large because the differential signal between possible Hamming weight measurements is, by assumption, small.

It is more experimentally advantageous to maximize the differential signal regardless of atom number, maximizing the resolvability of neighboring Hamming weights. Therefore, we may place the cavity on resonance with the $|1\rangle \leftrightarrow |e\rangle$ transition, which yields the bare cavity transmission spectrum if all atoms are in $|0\rangle$ and vacuum Rabi spectra with splitting $2g\sqrt{n_1}$ for Hamming weights n_1. The task of Hamming weight measurement is then the task

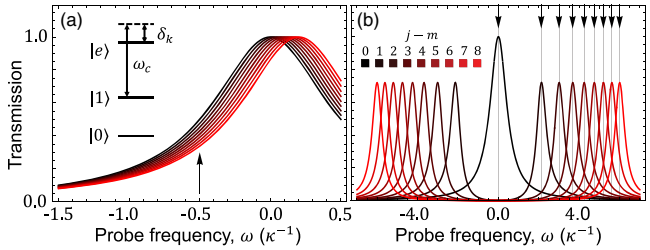

FIG. 4. Two schemes to experimentally implement Hamming weight measurements, illustrated for $n = 8$ qubits. (a) Probe on the side of fringe in the dispersive cavity regime, with photon counting in transmission to determine cavity shift magnitude. Inset: level diagram for our detection scheme. (b) Probe simultaneously at each possible resonance frequency in the resonant cavity regime, with heterodyne transmission detection to determine which frequency tone transmits.

of determining which of the possible spectra is realized by the cavity.

To this end, we propose a multichromatic probe laser with a spectral peak at each of the possible vacuum Rabi resonances, as depicted in Fig. 4(b), and power in each peak chosen to yield equal transmitted photon number. In the fully resolved limit, this laser probes each Hamming weight possibility in a time and with a number of transmitted photons that is independent of the total atom number. The frequency of the cavity transmission signal, which carries the desired Hamming weight information, may be revealed using standard optical heterodyne techniques.

The principal cost of this scheme is the requirement that the atom-cavity coupling g is $\Omega(\sqrt{n})$, to be able to resolve neighboring peaks that are $g\sqrt{n} - g\sqrt{n-1} \sim g/\sqrt{n}$ apart. Additionally, while not a fundamental limitation, the number of tones and bandwidth to produce the multichromatic probe laser and perform optical heterodyne measurement scale linearly with n. This scheme is also robust to a finite photon collection efficiency, as well as to imperfections due to a finite cooperativity; see Supplemental Material for details [74].

Outlook—We have shown an algorithm for preparing Dicke states with depth and width polylogarithmic in the number of qubits. The algorithm is compatible with existing experimental platforms, using only sequences of global single-qubit rotations and collective Hamming weight measurements. While our proposed implementation of Hamming weight measurements relies on uniform detunings across the atom ensemble, a natural extension is to relax the assumption that all atoms couple to the cavity equally, allowing for a richer class of measurements.

For example, we might extend our protocol by probing at the midpoint frequency to obtain a superposition of Dicke states $|j,m\rangle + |j,-m\rangle$, which have metrological applications [88].

Practically, the compatibility with near-term cavity systems and relatively small number of iterations can enable further improvements in sensitivity for emerging entanglement-based sensors, advancing the forefront of precision probes for fundamental science and metrology [63,64]. Combined with our proposed measurement scheme, this also offers a key benchmark for shallow-depth adaptive circuits in these systems.

Acknowledgments—We thank Jacob Lin for helpful discussions. J. Y., A. M. C., and A. V. G. were supported in part by the DOE ASCR Quantum Testbed Pathfinder program (Awards No. DE-SC0019040 and No. DE-SC0024220) and NSF QLCI (Award No. OMA-2120757). J. Y., A. M. C., and A. V. G. also acknowledge support from the U.S. Department of Energy, Office of Science, Accelerated Research in Quantum Computing, Fundamental Algorithmic Research toward Quantum Utility (FAR-Qu). J. Y. and A. V. G. were also supported in part by ARL (No. W911NF-24-2-0107), DARPA SAVaNT ADVENT, ARO MURI (Award No. W911NF1610349), NSF STAQ program, ONR MURI, AFOSR MURI, and NQVL:QSTD: Pilot:FTL. J. Y. and A. V. G. also acknowledge support from the U.S. Department of Energy, Office of Science, National Quantum Information Science Research Centers, Quantum Systems Accelerator (QSA). S. R. M. is supported by the NSF QLCI Grant No. OMA-2120757. Y.-X. W. acknowledges support from a QuICS Hartree Postdoctoral Fellowship. N. S. acknowledges support, in part, from ARO (No. W911NF-24-1-0064) and ARL (No. W911NF-24-2-0107).

Data availability—The data that support the findings of this article are openly available [89].

[1] R. H. Dicke, Phys. Rev. **93**, 99 (1954).
[2] P. W. Anderson, Phys. Rev. **86**, 694 (1952).
[3] H. J. Lipkin, N. Meshkov, and A. J. Glick, Nucl. Phys. **62**, 188 (1965).
[4] X.-Y. Luo, Y.-Q. Zou, L.-N. Wu, Q. Liu, M.-F. Han, M. K. Tey, and L. You, Science **355**, 620 (2017).
[5] A. S. Sørensen and K. Mølmer, Phys. Rev. Lett. **86**, 4431 (2001).
[6] R. Krischek, C. Schwemmer, W. Wieczorek, H. Weinfurter, P. Hyllus, L. Pezzé, and A. Smerzi, Phys. Rev. Lett. **107**, 080504 (2011).
[7] G. Tóth, Phys. Rev. A **85**, 022322 (2012).
[8] B. Lücke, M. Scherer, J. Kruse, L. Pezzé, F. Deuretzbacher, P. Hyllus, O. Topic, J. Peise, W. Ertmer, J. Arlt, L. Santos, A. Smerzi, and C. Klempt, Science **334**, 773 (2011).
[9] Z. Zhang and L. Duan, New J. Phys. **16**, 103037 (2014).
[10] F. Fröwis, M. Skotiniotis, B. Kraus, and W. Dür, New J. Phys. **16**, 083010 (2014).
[11] S. Altenburg, S. Wölk, G. Tóth, and O. Gühne, Phys. Rev. A **94**, 052306 (2016).
[12] Y. Ouyang, N. Shettell, and D. Markham, IEEE Trans. Inf. Theory **68**, 1809 (2022).

[13] Z. H. Saleem, M. Perlin, A. Shaji, and S. K. Gray, Phys. Rev. A **109**, 052615 (2024).
[14] A. M. Childs, E. Farhi, J. Goldstone, and S. Gutmann, Quantum Inf. Comput. **2**, 181 (2002).
[15] E. Farhi, J. Goldstone, and S. Gutmann, arXiv:1411.4028.
[16] S. Hadfield, Z. Wang, B. O'Gorman, E. G. Rieffel, D. Venturelli, and R. Biswas, Algorithms Mol. Biol. **12**, 34 (2019).
[17] J. Cook, S. Eidenbenz, and A. Bartschi, in *Proceedings of the 2020 IEEE International Conference on Quantum Computing and Engineering (QCE)* (IEEE, New York, 2020), 10.1109/QCE49297.2020.00021.
[18] S. P. Jordan, N. Shutty, M. Wootters, A. Zalcman, A. Schmidhuber, R. King, S. V. Isakov, and R. Babbush, Nature (London) **646**, 831 (2025).
[19] Y. Ouyang, Phys. Rev. A **90**, 062317 (2014).
[20] M. Plesch and V. Bužek, Phys. Rev. A **81**, 032317 (2010).
[21] J. S. Van Dyke, G. S. Barron, N. J. Mayhall, E. Barnes, and S. E. Economou, PRX Quantum **2**, 040329 (2021).
[22] G. Tóth, W. Wieczorek, D. Gross, R. Krischek, C. Schwemmer, and H. Weinfurter, Phys. Rev. Lett. **105**, 250403 (2010).
[23] R. Prevedel, G. Cronenberg, M. S. Tame, M. Paternostro, P. Walther, M. S. Kim, and A. Zeilinger, Phys. Rev. Lett. **103**, 020503 (2009).
[24] J. Preskill, Quantum **2**, 79 (2018).
[25] A. Bärtschi and S. Eidenbenz, in *Fundamentals of Computation Theory*, Lecture Notes in Computer Science, Vol. 11651 (Springer International Publishing, New York, 2019), pp. 126–139, 10.1007/978-3-030-25027-0_9.
[26] M. T. Johnsson, N. R. Mukty, D. Burgarth, T. Volz, and G. K. Brennen, Phys. Rev. Lett. **125**, 190403 (2020).
[27] Y. Wang and B. M. Terhal, Phys. Rev. A **104**, 032407 (2021).
[28] A. Bartschi and S. Eidenbenz, in *Proceedings of the 2022 IEEE International Conference on Quantum Computing and Engineering (QCE)* (IEEE, New York, 2022), 10.1109/QCE53715.2022.00027.
[29] S. Aktar, A. Bärtschi, A.-H. A. Badawy, and S. Eidenbenz, IEEE Trans. Quantum Eng. **3**, 1 (2022).
[30] H. Buhrman, M. Folkertsma, B. Loff, and N. M. P. Neumann, Quantum **8**, 1552 (2024).
[31] L. Piroli, G. Styliaris, and J. I. Cirac, Phys. Rev. Lett. **133**, 230401 (2024).
[32] D. Raveh and R. I. Nepomechie, Phys. Rev. A **110**, 052438 (2024).
[33] D. Raveh and R. I. Nepomechie, J. Phys. A **57**, 065302 (2024).
[34] R. I. Nepomechie, F. Ravanini, and D. Raveh, Adv. Quantum Technol. **7**, 2400057 (2024).
[35] N. Kiesel, C. Schmid, G. Tóth, E. Solano, and H. Weinfurter, Phys. Rev. Lett. **98**, 063604 (2007).
[36] W. Wieczorek, R. Krischek, N. Kiesel, P. Michelberger, G. Tóth, and H. Weinfurter, Phys. Rev. Lett. **103**, 020504 (2009).
[37] D. B. Hume, C. W. Chou, T. Rosenband, and D. J. Wineland, Phys. Rev. A **80**, 052302 (2009).
[38] T. Vanderbruggen, S. Bernon, A. Bertoldi, A. Landragin, and P. Bouyer, Phys. Rev. A **83**, 013821 (2011).
[39] K. Toyoda, T. Watanabe, T. Kimura, S. Nomura, S. Haze, and S. Urabe, Phys. Rev. A **83**, 022315 (2011).
[40] A. Chiuri, C. Greganti, M. Paternostro, G. Vallone, and P. Mataloni, Phys. Rev. Lett. **109**, 173604 (2012).
[41] A. Noguchi, K. Toyoda, and S. Urabe, Phys. Rev. Lett. **109**, 260502 (2012).
[42] F. Haas, J. Volz, R. Gehr, J. Reichel, and J. Estève, Science **344**, 180 (2014).
[43] B. Lücke, J. Peise, G. Vitagliano, J. Arlt, L. Santos, G. Tóth, and C. Klempt, Phys. Rev. Lett. **112**, 155304 (2014).
[44] T. Opatrný, H. Saberi, E. Brion, and K. Mølmer, Phys. Rev. A **93**, 023815 (2016).
[45] Y.-Q. Zou, L.-N. Wu, Q. Liu, X.-Y. Luo, S.-F. Guo, J.-H. Cao, M. K. Tey, and L. You, Proc. Natl. Acad. Sci. U.S.A. **115**, 6381 (2018).
[46] E. J. Davis, Z. Wang, A. H. Safavi-Naeini, and M. H. Schleier-Smith, Phys. Rev. Lett. **121**, 123602 (2018).
[47] S. C. Carrasco, M. H. Goerz, S. A. Malinovskaya, V. Vuletić, W. P. Schleich, and V. S. Malinovsky, Phys. Rev. Lett. **132**, 153603 (2024).
[48] L. Chen, L. Lu, L. Xia, Y. Lu, S. Zhu, and X.-S. Ma, Phys. Rev. Lett. **130**, 223601 (2023).
[49] L. J. Bond, M. J. Davis, J. Minář, R. Gerritsma, G. K. Brennen, and A. Safavi-Naini, Phys. Rev. Res. **7**, L022072 (2025).
[50] We are also aware of concurrent work by Liu, Childs, and Gottesman that also gives an algorithm for preparing Dicke states in $O(\log n)$ depth, using $O(n \log n)$ ancillae [51]. The approaches are very different: while we apply a simple sequence of collective rotations and collective J_z measurements, the other approach uses sorting networks. Our approach is simpler, likely performs better in practice, and can perform better when the Hamming weight is lower, while the other approach solves a more general symmetrization problem.
[51] Z. Liu, A. M. Childs, and D. Gottesman, arXiv:2411.04019.
[52] I. D. Leroux, M. H. Schleier-Smith, and V. Vuletić, Phys. Rev. Lett. **104**, 073602 (2010).
[53] M. H. Schleier-Smith, I. D. Leroux, and V. Vuletić, Phys. Rev. A **81**, 021804(R) (2010).
[54] S. L. Christensen, J.-B. Béguin, E. Bookjans, H. L. Sørensen, J. H. Müller, J. Appel, and E. S. Polzik, Phys. Rev. A **89**, 033801 (2014).
[55] W. Chen, J. Hu, Y. Duan, B. Braverman, H. Zhang, and V. Vuletić, Phys. Rev. Lett. **115**, 250502 (2015).
[56] K. C. Cox, G. P. Greve, J. M. Weiner, and J. K. Thompson, Phys. Rev. Lett. **116**, 093602 (2016).
[57] E. Deist, Y.-H. Lu, J. Ho, M. K. Pasha, J. Zeiher, Z. Yan, and D. M. Stamper-Kurn, Phys. Rev. Lett. **129**, 203602 (2022).
[58] J. Ramette, J. Sinclair, and V. Vuletić, arXiv:2401.11407.
[59] L. Hartung, M. Seubert, S. Welte, E. Distante, and G. Rempe, Science **385**, 179 (2024).
[60] B. Grinkemeyer, E. Guardado-Sanchez, I. Dimitrova, D. Shchepanovich, G. E. Mandopoulou, J. Borregaard, V. Vuletić, and M. D. Lukin, Science **387**, 1301 (2025).
[61] W. Zi, J. Nie, and X. Sun, IEEE Trans. Comput. Aided Des. Integr. Circuits Syst. **44**, 3060 (2025).
[62] S. Rethinasamy, M. L. LaBorde, and M. M. Wilde, Phys. Rev. A **110**, 052401 (2024).
[63] J. M. Robinson, M. Miklos, Y. M. Tso, C. J. Kennedy, T. Bothwell, D. Kedar, J. K. Thompson, and J. Ye, Nat. Phys. **20**, 208 (2024).

[64] T. Bothwell, C. J. Kennedy, A. Aeppli, D. Kedar, J. M. Robinson, E. Oelker, A. Staron, and J. Ye, Nature (London) **602**, 420 (2022).
[65] S. Kolkowitz, I. Pikovski, N. Langellier, M. D. Lukin, R. L. Walsworth, and J. Ye, Phys. Rev. D **94**, 124043 (2016).
[66] M. S. Safronova, D. Budker, D. DeMille, Derek F. Jackson Kimball, A. Derevianko, and C. W. Clark, Rev. Mod. Phys. **90**, 025008 (2018).
[67] J. Grotti *et al.*, Nat. Phys. **14**, 437 (2018).
[68] P. Wcisło *et al.*, Sci. Adv. **4**, eaau4869 (2018).
[69] T. E. Mehlstäubler, G. Grosche, C. Lisdat, P. O. Schmidt, and H. Denker, Rep. Prog. Phys. **81**, 064401 (2018).
[70] C. Sanner, N. Huntemann, R. Lange, C. Tamm, E. Peik, M. S. Safronova, and S. G. Porsev, Nature (London) **567**, 204 (2019).
[71] F. T. Arecchi, E. Courtens, R. Gilmore, and H. Thomas, Phys. Rev. A **6**, 2211 (1972).
[72] G. S. Agarwal, Phys. Rev. A **24**, 2889 (1981).
[73] J. P. Dowling, G. S. Agarwal, and W. P. Schleich, Phys. Rev. A **49**, 4101 (1994).
[74] See Supplemental Material at http://link.aps.org/supplemental/10.1103/9gjk-rgql for a rigorous proof of the logarithmic scaling and a discussion on the protocol's robustness to finite errors, which includes Refs. [75–81].
[75] D. A. Varshalovich, A. N. Moskalev, and V. K. Khersonskii, Wigner *d*-functions, in *Quantum Theory of Angular Momentum* (World Scientific, Singapore, 1988), Chap. 4, pp. 72–129, 10.1142/9789814415491_0005.
[76] R. Wong, Classical procedures, in *Asymptotic Approximations of Integrals*, Classics in Applied Mathematics No. 34 (SIAM, Philadelphia, 2001), Chap. 2, pp. 55–146, 10.1137/1.9780898719260.ch2.
[77] C. L. Siegel, Sitzungsber. Preuß. Akad. Wiss., Math.-Phys. Klasse **1**, 81 (1929).
[78] M. H. Schleier-Smith, I. D. Leroux, and V. Vuletić, Phys. Rev. Lett. **104**, 073604 (2010).
[79] K. Jacobs and D. A. Steck, Contemp. Phys. **47**, 279 (2006).
[80] L. B. Madsen and K. Mølmer, Phys. Rev. A **70**, 052324 (2004).
[81] J. Appel, P. J. Windpassinger, D. Oblak, U. B. Hoff, N. Kjærgaard, and E. S. Polzik, Proc. Natl. Acad. Sci. U.S.A. **106**, 10960 (2009).
[82] J. Kemeny and J. Snell, *Finite Markov Chains*, Finite Markov Chains (Van Nostrand, Princeton, 1960).
[83] J. Beugnon, C. Tuchendler, H. Marion, A. Gaëtan, Y. Miroshnychenko, Y. R. P. Sortais, A. M. Lance, M. P. A. Jones, G. Messin, A. Browaeys, and P. Grangier, Nat. Phys. **3**, 696 (2007).
[84] N. Schine, A. W. Young, W. J. Eckner, M. J. Martin, and A. M. Kaufman, Nat. Phys. **18**, 1067 (2022).
[85] S. Ma, A. P. Burgers, G. Liu, J. Wilson, B. Zhang, and J. D. Thompson, Phys. Rev. X **12**, 021028 (2022).
[86] H. Levine, D. Bluvstein, A. Keesling, T. T. Wang, S. Ebadi, G. Semeghini, A. Omran, M. Greiner, V. Vuletić, and M. D. Lukin, Phys. Rev. A **105**, 032618 (2022).
[87] G. Unnikrishnan, P. Ilzhöfer, A. Scholz, C. Hölzl, A. Götzelmann, R. K. Gupta, J. Zhao, J. Krauter, S. Weber, N. Makki, H. P. Büchler, T. Pfau, and F. Meinert, Phys. Rev. Lett. **132**, 150606 (2024).
[88] C.-J. Lin, Z.-W. Liu, V. V. Albert, and A. V. Gorshkov, Phys. Rev. Lett. **135**, 110801 (2025).
[89] J. Yu, Optimized rotation angles for preparing Dicke states, Zenodo, 2025, 10.5281/zenodo.17517248.
[90] M. Abramowitz and I. A. Stegun, *Handbook of Mathematical Functions*, Dover Books on Advanced Mathematics (Dover, 1972).

End Matter

Geometric argument—In this End Matter, we give the details of a geometric argument that Algorithm 1, as described in the main text, reaches the $|j, m_t\rangle$ Dicke state in $O[\log(j - m_t)]$ iterations. For completeness, we also include the pseudocode for Algorithm 2, which is the specialization of Algorithm 1 for $m_t = 0$ with the additional reset condition and whose run-time is proven in Supplemental Material [74].

We let $m_t \geq 0$ without loss of generality as the $m_t \leq 0$ case is symmetric via a global flip. For simplicity, we do not include a reset condition analogous to that in Algorithm 2, as it is not needed for our geometric argument.

We describe the expected behavior within the geometric picture, whose relevant quantities are shown in Fig. 5(a). The strategy is similar to the proof of Theorem 1. First, we use the geometric model to derive a coarse-grained expression for the transition probabilities in the large-j regime. Within this model, we compute the transition

ALGORITHM 2. Preparation of the $m_t = 0$ Dicke state using global rotations and J_z measurements.

```
Initialize 2j qubits each to |0⟩, m = j
while m ≠ 0 do
    Rotate by exp(−iθ_m J_y)
    m ← measure J_z
    if |m| > √j then
        Reset all qubits to |0⟩, m = j
```

ALGORITHM 1. Preparation of arbitrary $|j, m_t\rangle$ Dicke state using global rotations and J_z measurements.

```
Initialize 2j qubits each to |0⟩, m = j
while m ≠ m_t do
    Rotate by exp(−iθ_{m_t,m} J_y), where θ_{m_t,m} = arcsin[(m r_{m_t} − m_t r_m)/r_0^2]
    m ← measure J_z
```

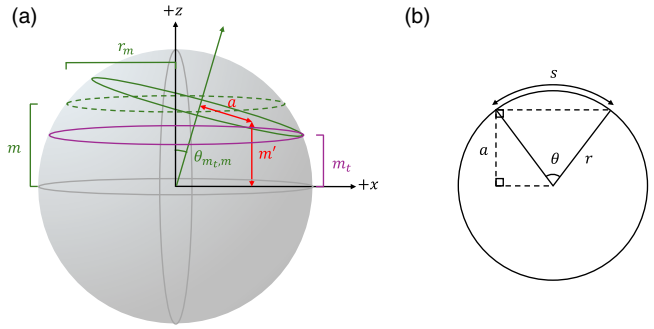

FIG. 5. (a) Geometry of the (rotated) Dicke states, idealized as rings on the collective Bloch sphere, corresponding to the large-j limit of the Husimi Q distribution. We show the ring corresponding to $|j,m\rangle$ (green) before (dotted) and after (solid) a rotation by an angle $\theta_{m_t,m}$. We also show the ring for the corresponding target state $|j,m_t\rangle$ (purple). Other variables m' and a used in our calculation of the probability distribution function are shown in red. (b) A two-dimensional cross section of a Dicke ring with the relevant parameters for calculating arc length.

probabilities $\mathrm{Prob}[m \to m']$ as the overlap of the Q distribution ring of $|j,m'\rangle$ with the rotated ring from $|j,m\rangle$. Then we show that, for some constant $\alpha > 0$, the expected deviation $\langle (m'-m_t)^\alpha \rangle$ decays exponentially in time. The conclusion then follows in the same manner.

We begin by computing the arc length of a circular segment a distance a from the center of a ring of radius r, as shown in Fig. 5(b). This is equivalently described by the arc length of the circular sector of angular width θ, defined such that $\cos(\theta/2) = a/r$. The corresponding arc length is then $s = 2r\arccos(a/r)$, and we have the (unsigned) infinitesimal arc length

$$\mathrm{d}s = \frac{2\mathrm{d}a}{\sqrt{1-(a/r)^2}}. \tag{A1}$$

Now, consider a horizontal ring at height m above the origin (with radius r_m) and rotated by an angle $\theta_{m_t,m}$ about $+y$ so that the bottom edge of the rotated ring lies at height m_t; $\theta_{m_t,m}$ is defined via Eq. (2). For the differential arc length of this rotated ring, we have the relation $a = (m'-m_t)/\sin\theta_{m_t,m} - r_m$, so

$$\mathrm{d}s = \frac{2r_m \mathrm{d}m'}{(m'-m_t)\sqrt{2r_m \sin\theta_{m_t,m}/(m'-m_t) - 1}}. \tag{A2}$$

This expression is defined in the range $m_t < m' < m_t + 2r_m \sin\theta_{m_t,m}$.

In the large-j limit, where the Q distribution of the state $e^{-i\theta_{m_t,m}J_y}|j,m\rangle$ is well represented by this tilted ring, we assume that the probability to obtain $J_z = m'$ is proportional to the arc length lying between m' and $m'+dm'$. Properly normalizing, we thus have the continuous probability distribution function (PDF)

$$p(m',m;m_t) = \frac{1}{\pi r_m \sin\theta_{m_t,m}\{[(m'-m_t)/(r_m\sin\theta_{m_t,m})][2-(m'-m_t)/(r_m\sin\theta_{m_t,m})]\}^{1/2}} \tag{A3}$$

for $m_t < m' < m_t + 2r_m \sin\theta_{m_t,m}$ and assume zero probability for m' outside this range. We note that, while the integral of this expression converges, the PDF diverges at m_t and $m_t + 2r_m$. This indicates that the overlap probability is maximal at these points, and we thus utilize the set of rotation angles $\theta_{m_t,m}$ for preparing target Dicke states $|j,m_t\rangle$.

This offers a coarse-grained way to predict moments of J_z. In particular, Eq. (A3) takes the form of a beta distribution, with moments

$$\langle (m'-m_t)^\alpha | m\rangle = \int_{m_t}^{m_t+2r_m\sin\theta_{m_t,m}} (m'-m_t)^\alpha p(m',m;m_t)\mathrm{d}m' \tag{A4}$$

$$= \frac{B(\alpha+1/2,1/2)}{\pi}(2r_m\sin\theta_{m_t,m})^\alpha \tag{A5}$$

for beta function $B(x,y) = \Gamma(x)\Gamma(y)/\Gamma(x+y)$ and gamma function $\Gamma(x)$. Here, $\langle (m'-m_t)^\alpha|m\rangle$ is the expectation of $(m'-m_t)^\alpha$, conditional on the previous state being $|j,m\rangle$.

For $0 < \alpha < 1$, we have $\langle (m'-m_t)^\alpha|m\rangle < c(m-m_t)^\alpha$ for some j-independent constant $0 < c < 1$. To see this, we first note that

$$\frac{B(\alpha+1/2,1/2)}{\pi}\left(\frac{2r_m\sin\theta_{m_t,m}}{m-m_t}\right)^\alpha \le \frac{B(\alpha+1/2,1/2)}{\pi}2^\alpha, \tag{A6}$$

using the fact that $r_0 \ge r_{m_t} \ge r_m$ for all m such that $m \ge m_t$, $m \le j$. Now let $f(\alpha) = \ln[B(\alpha+1/2,1/2)2^\alpha/\pi]$. We have $f''(\alpha) = \psi^{(1)}(\alpha+1/2) - \psi^{(1)}(\alpha+1)$, where $\psi^{(n)}(\alpha) = d^{(n+1)}\ln\Gamma(\alpha)/d^{(n+1)}\alpha$ is the polygamma function of order n. From the series representation $\psi^{(n)}(\alpha) = (-1)^{n+1}n!\sum_{k=0}^{\infty}(\alpha+k)^{-(n+1)}$ [90], we see that $\psi^{(1)}(\alpha)$ is strictly decreasing for all $\alpha > 0$, since $\psi^{(2)}(\alpha) < 0$. This implies that $f''(\alpha) > 0$, so $f(\alpha)$ is convex for $\alpha > 0$. Now, $f(0) = 0$ and $f(1) = 0$, so for $0 < \alpha < 1$ we have $f(\alpha) < 0$ and the right-hand side of Eq. (A6) is strictly upper bounded by 1. For any fixed α in this range, we may

therefore select a (j-independent) constant $c < 1$ such that Eq. (A5) is strictly upper bounded by $c(m - m_t)^\alpha$.

Thus, $\langle (m' - m_t)^\alpha \rangle$ decays by a factor of c at each step of Algorithm 1. Let $\langle (m' - m_t)^\alpha \rangle_k$ denote the expectation after k steps. We initially have $\langle (m' - m_t)^\alpha \rangle_0 = (j - m_t)^\alpha$, so by induction $\langle (m' - m_t)^\alpha \rangle_k < c^k (j - m_t)^\alpha$. Now, if we require $\langle (m - m_t)^\alpha \rangle_n < \varepsilon$ for some $\varepsilon > 0$, this can be achieved in

$$n > \frac{\alpha \ln(j - m_t) + \ln(1/\varepsilon)}{\ln(1/c)} \tag{A7}$$

steps, or $n = O[\log(j - m_t)]$, as claimed.